General Disclaimer

One or more of the Following Statements may affect this Document

- This document has been reproduced from the best copy furnished by the organizational source. It is being released in the interest of making available as much information as possible.

- This document may contain data, which exceeds the sheet parameters. It was furnished in this condition by the organizational source and is the best copy available.

- This document may contain tone-on-tone or color graphs, charts and/or pictures, which have been reproduced in black and white.

- This document is paginated as submitted by the original source.

- Portions of this document are not fully legible due to the historical nature of some of the material. However, it is the best reproduction available from the original submission.

CR-86255

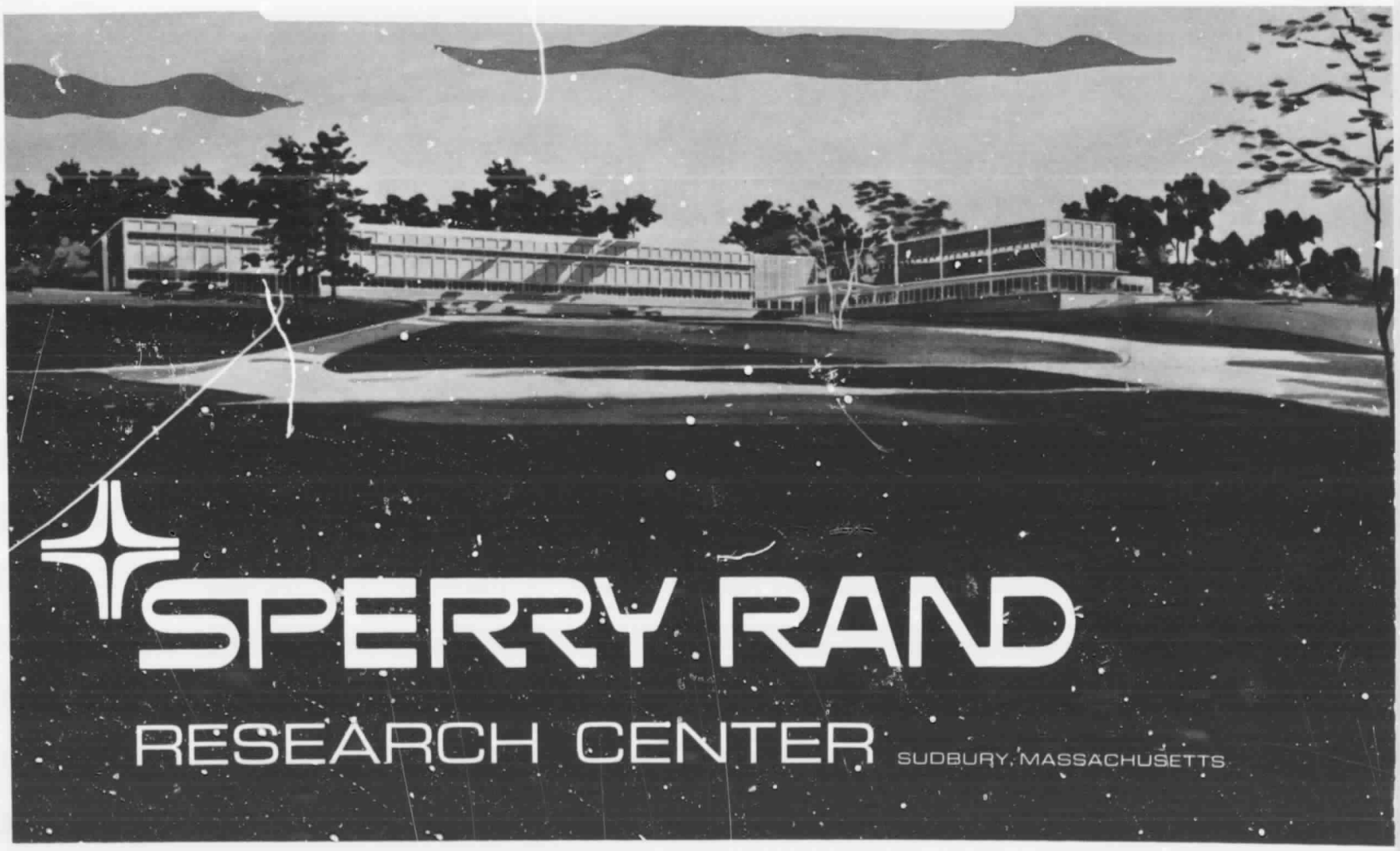

SPERRY RAND
CORPORATION

SRRC-CR-69-16

June 1969

SEVENTH QUARTERLY TECHNICAL REPORT
INVESTIGATION OF NEW CONCEPTS
OF ADAPTIVE DEVICES

Contract No. NAS 12-570

Period Covered:

3 March 1969 - 2 June 1969

E. Lewis, F. Sewell, H. A. R. Wegener
Sperry Rand Research Center, Sudbury, Massachusetts

June 1969

Prepared for

NASA Electronics Research Center
Cambridge, Massachusetts

SPERRY RAND RESEARCH CENTER
SUDBURY, MASSACHUSETTS 01776

TABLE OF CONTENTS

LIST OF ILLUSTRATIONS

ANALYSIS OF CHARGE DECAY IN THE MI_2I_1S MEMORY DEVICE

1. Introductory Comments

The previous two letter reports have been concerned with the charging characteristics of the memory device both at 24°C and at 150°C. It was shown that at these two temperatures the two conduction mechanisms involved in the charge storage process are tunneling and Poole-Frenkel conduction. This was quantitatively confirmed on the basis of static and transient charging measurements. The persistence of this stored charge is of fundamental importance since it is the property that yields the memory effect.

The problem of predicting charge decay in the present memory device is one that depends on several factors. These include the polarity of the stored charge, the conduction mechanisms involved in the relaxation of this charge, and the distribution of the stored charge. In the simplest configuration charge is stored at a well defined interface between regions of different conductivity. If the location of this interface is known along with the charge transfer mechanisms, then the decay can be accurately predicted. However, the case that generally prevails is one of an interface that is either not well defined or does not exist, as in the case of a charge distribution. The interface tunneling mechanism is also not well defined. It depends on the trap depth and density in the silicon nitride, whether or not a trap distribution exists between a thin oxide layer and the deposited nitride, and the direction of charge transfer.

As an illustration, consider the structure shown in Fig. 1. This structure consists of two regions with different conduction mechanisms separated by a well-defined interface at which the charge storage occurs. When the negative gate bias is applied as shown, the fields established in both regions are in the same direction. For this structure I_1 has been assumed to be more conductive than I_2. After the bias is removed, the field in I_1 is reversed. Since the charge transfer rates for I_1 are those shown in Fig. 1c, the decay through I_1 occurs following a conduction characteristic different from that during the charging process. It is important to note

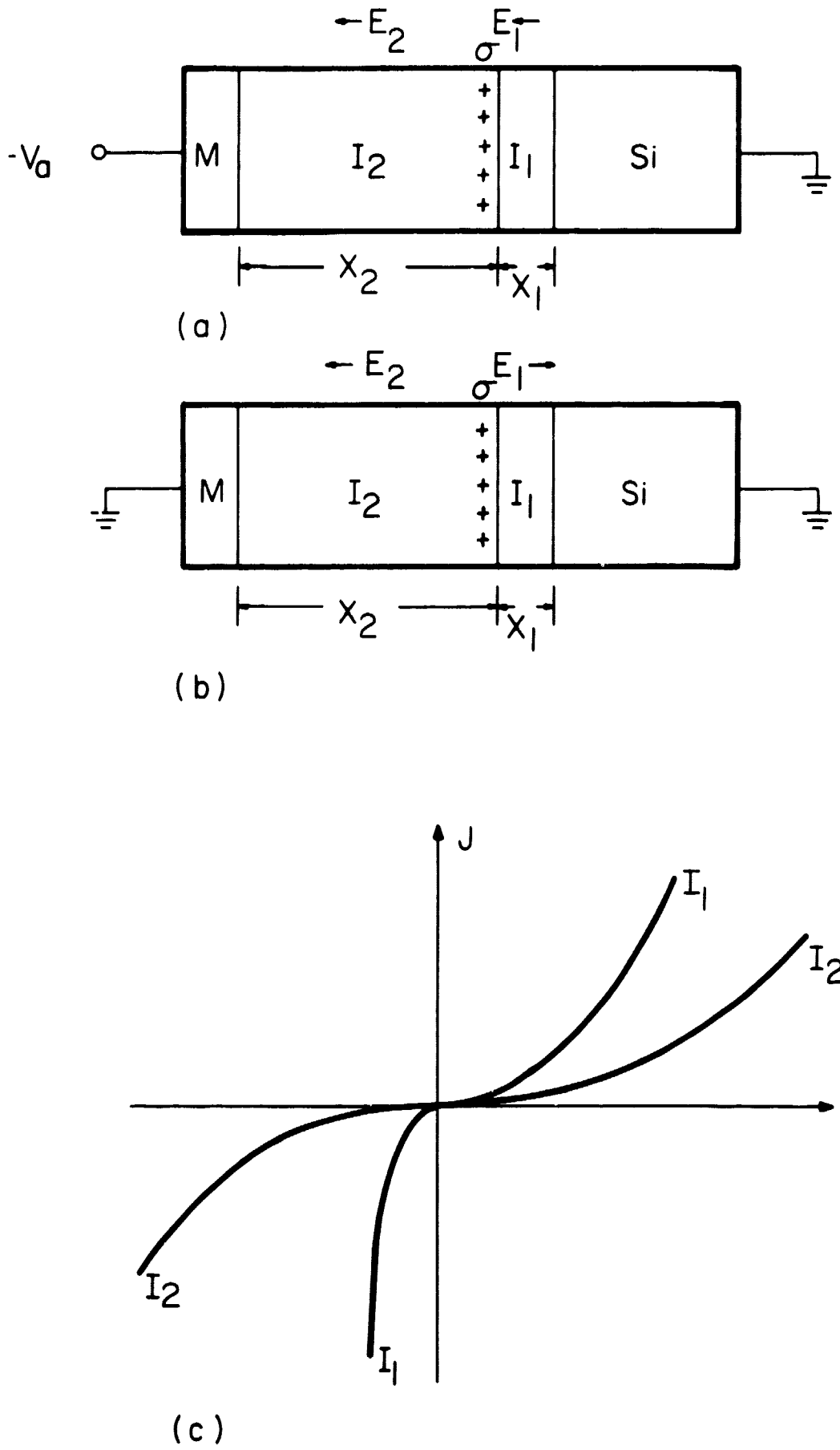

FIG. 1 Field conditions in a memory structure with a well-defined interface before and after the application of a negative charging voltage. For this structure I_1 is the more conductive layer.

(a) Fields in both regions are in the same direction when the bias is applied.

(b) The field in I_1 reverses after the charging voltage is removed.

(c) J vs E characteristics for I_1 and I_2. (I_1 is not symmetric; I_2 is symmetric.)

that for a device of this type it is most efficient to charge on the more conductive I_1 curve so that the discharge occurs along the less conductive portion.

A more complex situation exists when the charge is distributed over an extended range. This is illustrated in Fig. 2. In this figure two charge transfer rates, J_1 and J_2, have been shown. For illustration, J_1 is greater than J_2 and positive charge is being stored. The analysis of the decay process for a distributed charge of positive polarity will be presented in the following sections along with that for a charge sheet. The analysis of negative stored charges will be treated in the future.

2. Decay of a Charge Sheet

In any decay analysis the detailed conduction laws for all the charge transfer processes must be known. Referring to the structure shown in Fig. 1 along with the known conduction characteristics one may establish the mathematical relations necessary to predict its decay behavior. For simplicity consider that a bias has been applied long enough so that an equilibrium condition has been reached.

$$J_1 = J_2 = J_{eq}$$

$$\sigma_o = \epsilon_1 E_{1s} - \epsilon_2 E_{2s} \qquad (1)$$

$$V_a = E_{1s} x_1 + E_{2s} x_2$$

These equations follow from current continuity, Gauss' law, and Ohm's law, respectively.

When the excitation is removed, the internal fields adjust themselves instantaneously to account for the fact that $V_a = 0$ and σ_o is initially unchanged (i.e. at $t = 0^+$, $V_a = 0$, and $\sigma = \sigma_o$).

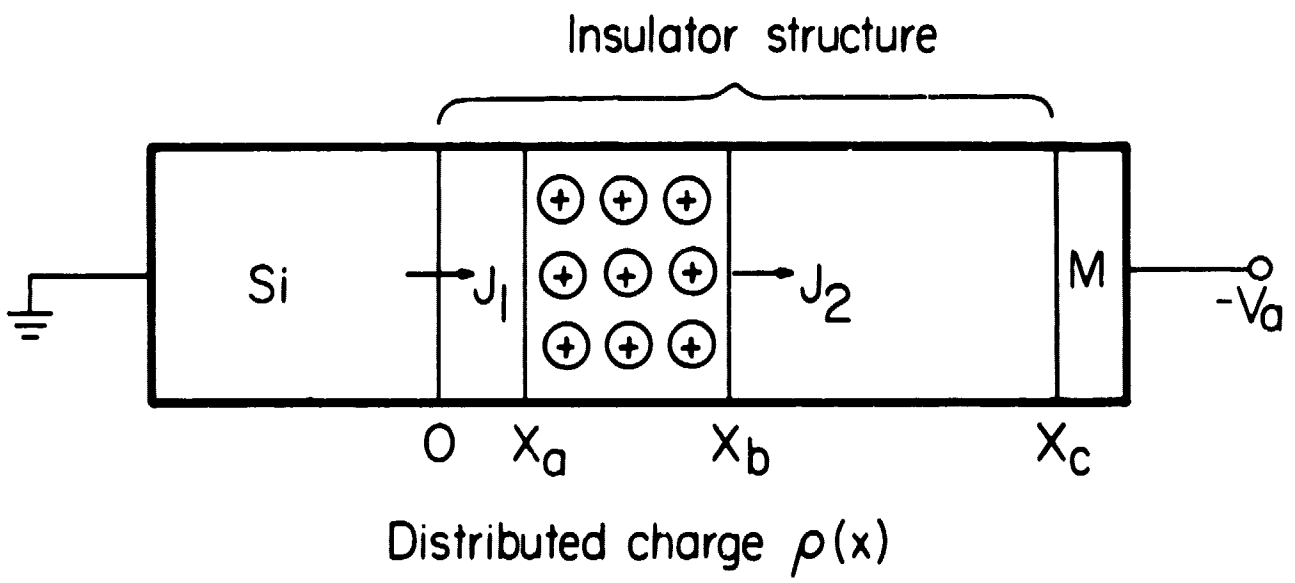

FIG. 2 Volume distribution of stored charge in a memory device.

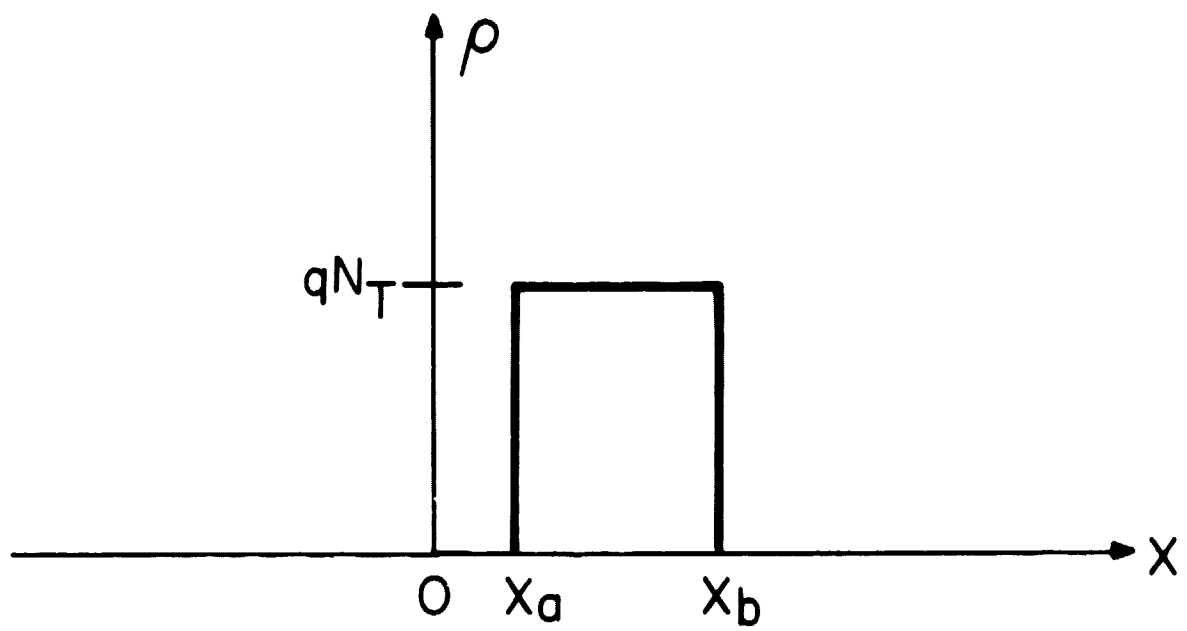

FIG. 3 Assumed charge distribution stored in gate structure of a memory device.

Therefore, at $t = 0^+$ Gauss' law and Ohm's law become

$$\sigma_0 = \epsilon_1 E_{10} - \epsilon_2 E_{20}$$
$$0 = x_1 E_{10} + x_2 E_{20} \tag{2}$$

From these equations the initial fields may be determined

$$E_{20} = \frac{-\sigma_0}{\epsilon_1 \frac{x_2}{x_1} + \epsilon_2}$$
$$E_{10} = \frac{\frac{x_2}{x_1}\sigma_0}{\epsilon_1 \frac{x_2}{x_1} + \epsilon_2} \tag{3}$$

The stored charge, σ_0, will decay at a rate governed by the current continuity equation

$$J_1 + J_2 = -\frac{\partial \sigma}{\partial t} \tag{4}$$

where J_1 and J_2 are the charge transfer rates. Recall that J_1 for charging is not equivalent to that during the discharge process.

From Eq. (4) the decay time may be solved.

$$t = \frac{-d\sigma}{J_1 + J_2} \tag{5}$$

Using Gauss' law the charge can be related to the fields.

$$\sigma = \epsilon_1 E_1 - \epsilon_2 E_2 \tag{6}$$

Then

$$d\sigma = \epsilon_1 dE_1 - \epsilon_2 dE_2 \tag{7}$$

Also, since $V_a = 0$, Ohm's law can be used to relate E_1 and E_2.

$$E_1 = - \frac{x_2}{x_1} E_2 \tag{8}$$

Therefore, Eq. (5) becomes

$$t = \frac{(\epsilon_2 + \epsilon_1 \frac{x_2}{x_1}) \, dE_2}{J_1 + J_2} \tag{9}$$

This can be further analytically simplified by using the fact that, in present device structures, J_1 can be described by a Fowler-Nordheim tunnel equation of the form

$$J_1 = J_{o1} \epsilon^{-E_0/E_1} \tag{10}$$

and J_2 can be described by a Poole-Frenkel equation of the form

$$J_2 = J_{o2} \epsilon^{a\sqrt{E_2}} \tag{11}$$

In these equations J_{0_1}, J_{0_2}, E_0, and a can be graphically determined. Therefore, by combining Eqs. (8), (9), (10), and (11) we have

$$t = \int_{E_{20}}^{0} \frac{(\epsilon_2 + \epsilon_1 \frac{x_2}{x_1}) \, dE_2}{J_{o1} \epsilon^{\frac{-E_0 x_1}{E_2 x_2}} + J_{o2} \epsilon^{a\sqrt{E_2}}} \tag{12}$$

This equation cannot be solved by any direct closed form integration. However, depending on the values of the various parameters in the denominator, one of the terms may be dominant. If either the Poole-Frenkel term or the Fowler-Nordheim term is neglected then a rather simple series solution is obtainable. This solution should apply for a device having a well defined oxide-nitride interface with electronic trap densities in excess of $10^{10}/cm^2$.

If one is interested in the rate of charge decay during interrogation of the device it is a simple matter to superimpose an external field in the equations leading to the solution shown in Eq. (12).

3. Decay of a Charge Distribution

In order to mathematically describe the decay of a charge distribution stored in the gate structure of a memory device, a description of this distribution must be available. A way of arriving at a plausible detailed description of this charge distribution is to consider the actual charging process. The charging process that will be considered consists of establishing a positive charge distribution resulting from the difference in charge transfer rates that can be described by the processes discussed in the last section. The tunneling process involves that of charge transfer directly from filled levels in the nitride into the nitride conduction band and then into the silicon. The extent of the uncovered charge resulting from this process is a function of the density of available filled levels, the depth of such levels, and the lifetime of carriers in the nitride. Quantities such as lifetime and trap density are certainly related. Therefore, a reasonable representation of the stored positive charge in the nitride is shown in Fig. 3. The spatial parameters are equivalent to those shown in Fig. 2. The charge density is assumed to be constant over a defined region from $x = x_a$ to $x = x_b$. The magnitude of the charge density is equivalent to that of the uniformly charged trap distribution. The existence of a neutral region from $x = 0$ to $x = x_a$ can arise from the existence of a trap free interface layer, such as silicon oxide.

The process of decay will consist of filling these uncovered charge centers by transferring charge from neutral regions in the silicon nitride or from the silicon across the energy barrier existing between insulator conduction band and that of the silicon. After the charge has been established and the external field removed, the internal field and potential distribution can be determined by solving Poisson's equation with the appropriate boundary conditions.

$$\frac{d^2V}{dx^2} = -\frac{\rho}{\epsilon} \tag{13}$$

There will be three potential field solutions:

$$V_1 \text{ for } 0 \leq x \leq x_a$$

$$V_2 \text{ for } x_a \leq x \leq x_b$$

$$V_3 \text{ for } x_b \leq x \leq x_c$$

The boundary conditions for these solutions are

$$\text{at } x = 0;\ V_1 = 0 \qquad \text{at } x = x_c;\ V_3 = 0$$

$$\text{at } x = x_a;\ V_1 = V_2 \qquad \text{at } x = x_b;\ V_2 = V_3$$

$$\frac{\partial V_1}{\partial x} = \frac{\partial V_2}{\partial x} \qquad \frac{\partial V_2}{\partial x} = \frac{\partial V_3}{\partial x}$$

After solving Eq. (13) with the appropriate boundary conditions applied we have

$$V_1 = \frac{\rho}{\epsilon}\left[(x_b - x_a) - \frac{(x_b^2 - x_a^2)}{2x_c}\right] x \qquad (14)$$

$$V_2 = -\frac{\rho}{2\epsilon} x^2 + \frac{\rho}{\epsilon}\left[x_b - \frac{(x_b^2 - x_a^2)}{2x_c}\right] x - \frac{\rho}{2\epsilon} x_a^2 \qquad (15)$$

$$V_3 = -\frac{\rho}{2\epsilon}\frac{(x_b^2 - x_a^2)}{x_c} x + \frac{\rho}{2\epsilon}(x_b^2 - x_a^2) \qquad (16)$$

In these solutions the same permittivity ϵ has been used. This is done primarily for simplicity. Clearly, the expression for V_1 and V_3 would not be affected by assigning permittivities of ϵ_1 and ϵ_2 to them. In practice, V_2 will be over a region having a permittivity either entirely ϵ_1 or a permittivity entirely ϵ_2. However, even if there were two different permittivites in the region bounded by x_a and x_b, the subdivision of this region into two with a single permittivity would not raise the complexity of the system to an undue extent.

Now from these potential solutions, the electrical fields may be determined by calculating the gradients of the potentials.

$$E_1 = -\frac{\partial V_1}{\partial x} = -\frac{\rho}{\epsilon}\left[(x_b - x_a) - \frac{(x_b^2 - x_a^2)}{2x_c}\right] \tag{17}$$

$$E_2 = -\frac{\partial V_2}{2x} = \frac{\rho}{\epsilon}x - \frac{\rho}{\epsilon}x_b - \frac{(x_b^2 - x_a^2)}{2x_c} \tag{18}$$

$$E_3 = -\frac{\partial V_3}{\partial x} = \frac{\rho}{2\epsilon}\frac{(x_b^2 - x_a^2)}{x_c} \tag{19}$$

A sketch of these electric fields is shown in Fig. 4. There are no numerical values given for either the distance parameter x or the magnitude of the fields. The important features to observe from this sketch are the field directions and the fact that the magnitudes of the fields are the greatest outside the space charge. The latter feature is important in describing the decay process. This process involves the transfer of electrons from the silicon into the charged region of the nitride and the transfer of electrons from the metal electrode through the neutral region of the nitride into the space charge. As soon as the electrons enter the space charge the field starts to decrease, as exemplified by the sketch shown in Fig. 4. Therefore, the incoming electrons will neutralize the uncovered positive charge within a short distance after entering the space charge. This will result in a reduced space charge width, whose rate of reduction is a function of the charge transfer rates of the incoming electrons.

A useful sketch is that of the energy band deformation of the nitride conduction band due to the presence of this space charge. This is shown in Fig. 5. This is obtained by superimposing the potential field solutions (Eqs. (14), (15), and (16)) on the neutral energy band diagram of the silicon-silicon nitride structure. The rate of charge decay can be related to the charge transfer rates through the current continuity equation

$$-\frac{d\sigma}{dt} = J_1 + J_3 \tag{20}$$

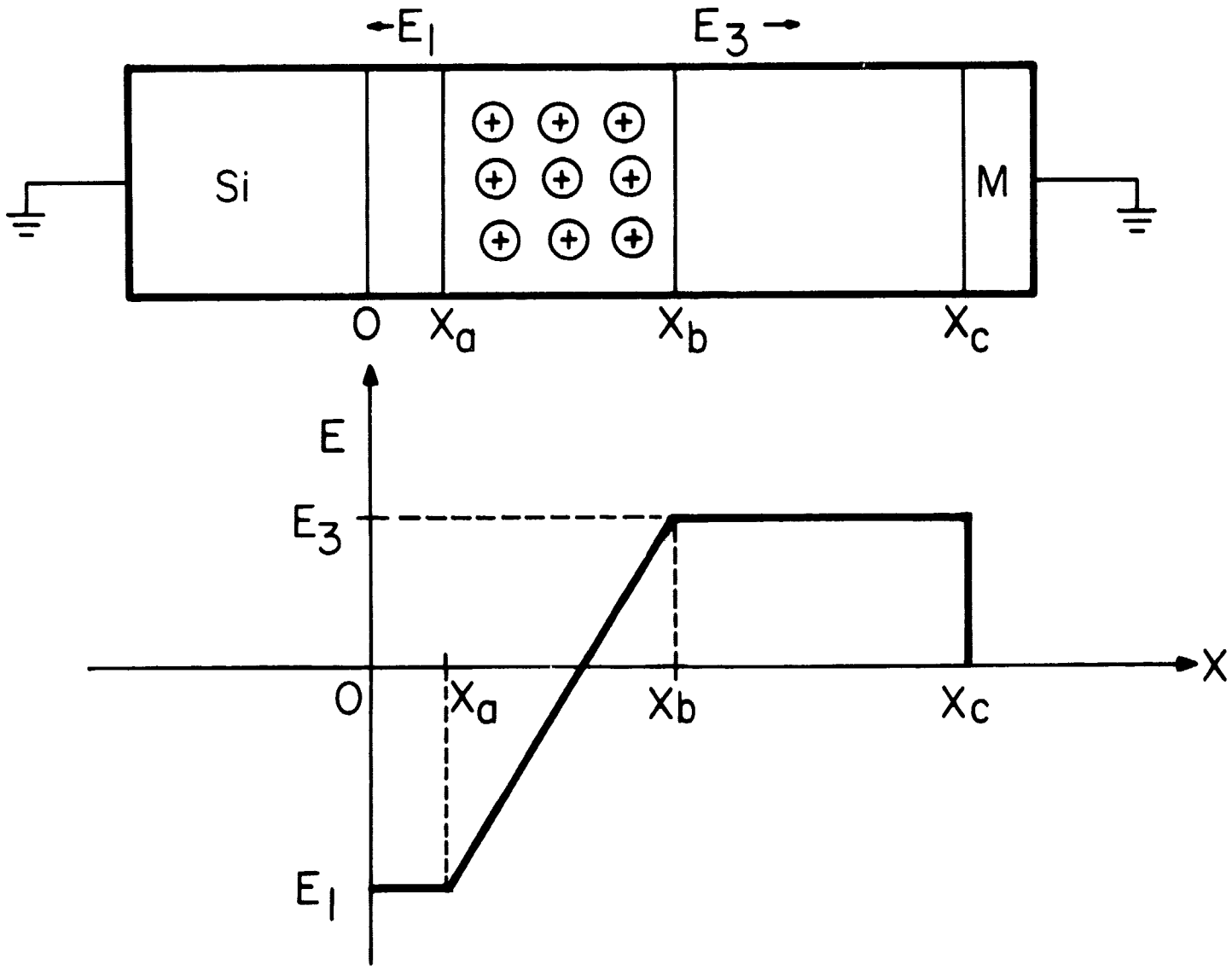

FIG. 4 Electric field distribution in the gate structure of a memory device with a defined uniform distribution of charge.

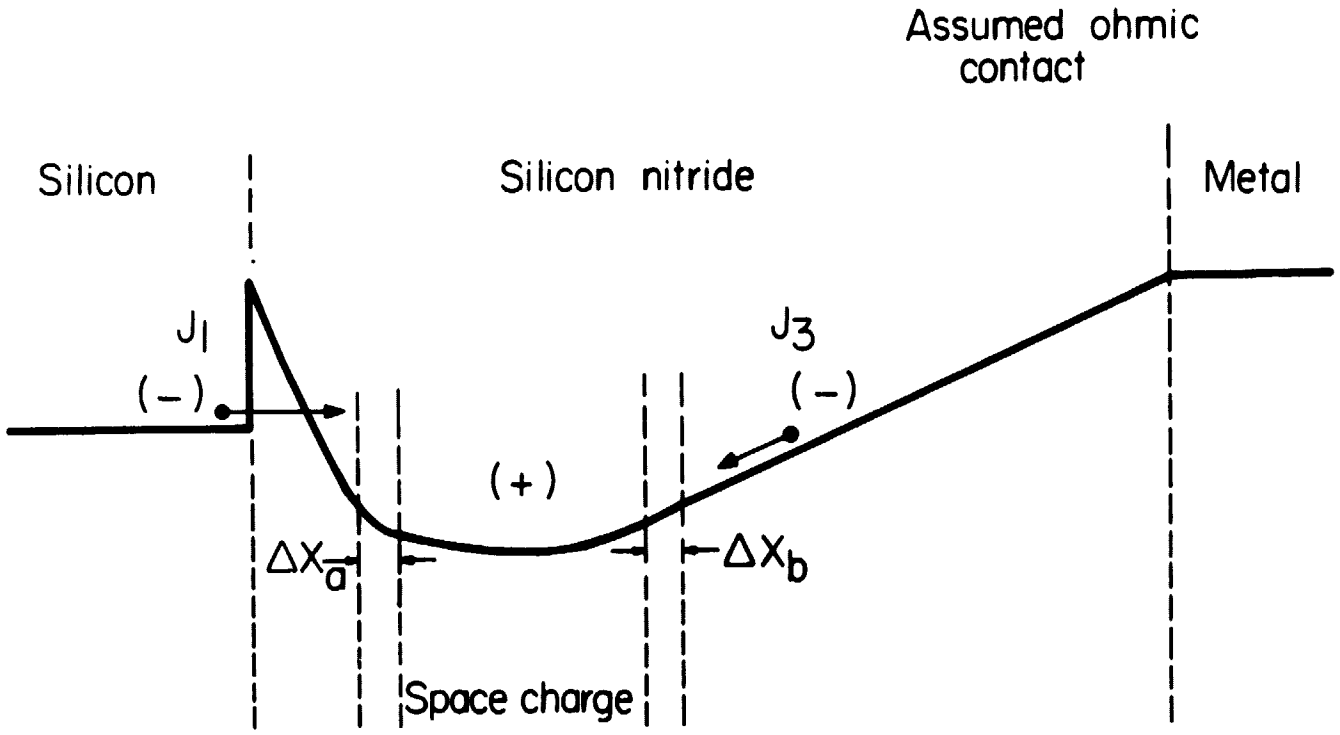

FIG. 5 Energy band diagram of MNS structure with stored distributed charge (not to scale). For simplicity only the conduction band edge has been shown. The effect of electron motion on the decay of this charge is also shown.

In terms of the present charge system

$$\sigma = \rho(x_b - x_a) \tag{21}$$

and

$$\frac{d\sigma}{dt} = \rho\left(\frac{dx_b}{dt} - \frac{dx_a}{dt}\right) \tag{22}$$

Therefore, by combining Eqs. (20) and (22) we have

$$J_1 + J_3 = -\rho\left(\frac{dx_b}{dt} - \frac{dx_a}{dt}\right) \tag{23}$$

We can observe from Eq. (22) that this represents the reduction of the edges of the space charge region. The solution to Eq. (22) is rather complex in that J_1 and J_3 are related to their respective fields by the following equations:

$$J_1 = J_{01}\epsilon^{-E_0/E_1} \tag{24}$$

$$J_3 = J_{03}\epsilon^{a\sqrt{E_3}}$$

The fields E_1 and E_3 are related to the spatial parameters x_a and x_b through Eqs. (17) and (19). Reducing Eq. (23) to one spatial variable must be accomplished through the use of Ohm's law.

$$0 = E_1 x_a + E_3(x_a - x_b) + \int_{x_a}^{x_b} E_2\,dx \tag{25}$$

Instead of attempting this solution, a very advantageous simplification can be obtained by noting that since the charge transfer rate from the silicon into the space charge is governed by a tunneling process, self-limiting occurs. This is so because as the space is neutralized the tunnel barrier width increases with a corresponding decrease in the field. Therefore, the remainder

of the decay process is governed primarily by the flow of electrons through the nitride (region 3). For initial space charge widths in the range of 200 to 300 angstroms this self-limiting will occur early in the decay process. Tunnel barrier widths much in excess of 50 angstroms do not allow for the transfer of an appreciable amount of charge. By neglecting the initial decay resulting from the charge transfer from the silicon we may write

$$- \frac{d\sigma}{dt} = J_3 = - \rho \frac{dx}{dt} \tag{26}$$

Then the decay time may be solved for

$$t = \int_{x_b}^{x_a} \rho \frac{dx}{J_3} \tag{27}$$

where

$$\rho = qN_T \tag{28}$$

and

$$J_3 = J_{o3}\, e^{a\sqrt{E_3}} \tag{29}$$

Using the solution for E_3 shown in Eq. (19), where x_b is the variable, and Eqs. (28) and (29), the time solution becomes

$$t = - \int_{x_b}^{x} \frac{q\, N_T dx}{J_{o3}\, e^{a \sqrt{\frac{qN_T}{2\epsilon x_c}(x^2 - x_a^2)}}} \tag{30}$$

One further simplification can be obtained if $x_b \gg x_a$; this is to let $x_a \to 0$. Then,

$$t = -\int_{x_b}^{x} \frac{qN_T}{J_{o3}} \epsilon^{-a\sqrt{\frac{qN_T}{2\epsilon x_c}}\,x}\,dx \tag{31}$$

This is readily solved to yield

$$t = \frac{qN_T}{mJ_{o3}}\left[\epsilon^{-mx} - \epsilon^{-mx_b}\right] \tag{32}$$

where

$$m = a\sqrt{\frac{qN_T}{2\epsilon x_c}}$$

4. MNS Light Sensitive Memory Element

This section describes a new device which can detect and store an optical signal. This device is an MNS-VTT utilized in a new manner that makes its operation sensitive to light. The principal advantage of this device is that it combines the light detecting mechanism and the storage mechanism into one. Heretofore, image storage schemes required one device to detect light, such as a reversed biased p-n junction, and another device to store the detected data, such as a capacitor or some other storage circuit. This device has, in addition, all the advantages of the MNS-VTT: LSI compatibility, non-volatile storage, nondestructive readout. A third feature of the MNS-VTT light sensing memory element is that, depending on the memory interrogation scheme, it may be used either in a digital or an analog manner. For example an element of an array can be interrogated with a fixed voltage to sense either an ON or OFF condition corresponding to a light or dark condition during write. On the other hand, an element of an array may be interrogated to determine its V_T, which will have been set to a value corresponding directly to the intensity of light incident on it during the writing cycle.

The structure and operation of the MNS-VTT light sensing memory element are shown in Fig. 6. While the device (under the proper operating conditions) is light sensitive using an opaque gate electrode, its sensitivity to light is greatly enhanced by the use of the transparent material. The primary requirement for light sensitive operation is that the source and drain be isolated from ground (floating) during the write cycle. This is shown in Fig. 6. If either or both the source and drain are grounded during the write cycle, the light will not affect the behavior of the device.

The operating of the MNS-VTT light sensing memory element may be understood by considering the effect of the silicon space charge region beneath the MNS gate. Under certain circumstances a large voltage drop may occur in the space charge region, reducing the voltage across the insulator and therefore inhibiting or delaying the charging process. The conditions are as follows; The polarity of the applied voltage must be such as to tend to create an inversion region in the silicon substrate. Thus a negative voltage is required for an n-type substrate and a positive voltage is required for a p-type substrate. The second condition, pointed out previously, is that the source and drain regions must be unconnected, that is, floating. Under these conditions the application of the writing voltage will sweep out the majority carriers from beneath the gate and thus form a space charge region. With the source and drain regions floating, there is no external source of minority carriers to form an inversion layer. Thus the field lines from the gate electrode must terminate on the donor or acceptor sites in the bulk silicon, forming a space charge region across which a considerable voltage may be dropped. Then the applied voltage is no longer entirely dropped across the insulator, but divided between the insulator and the space charge. The rate at which the space charge voltage is reduced depends on the rate at which minority carriers are generated in the space charge region and are swept to the silicon-insulator interface. As this process takes place, more and more field lines can terminate on the inversion layer that is forming so that the space charge voltage is reduced. Thus the time it takes to reduce the space charge voltage and thereby increase the insulator voltage is related to the time that the charging process is delayed. But the rate at which

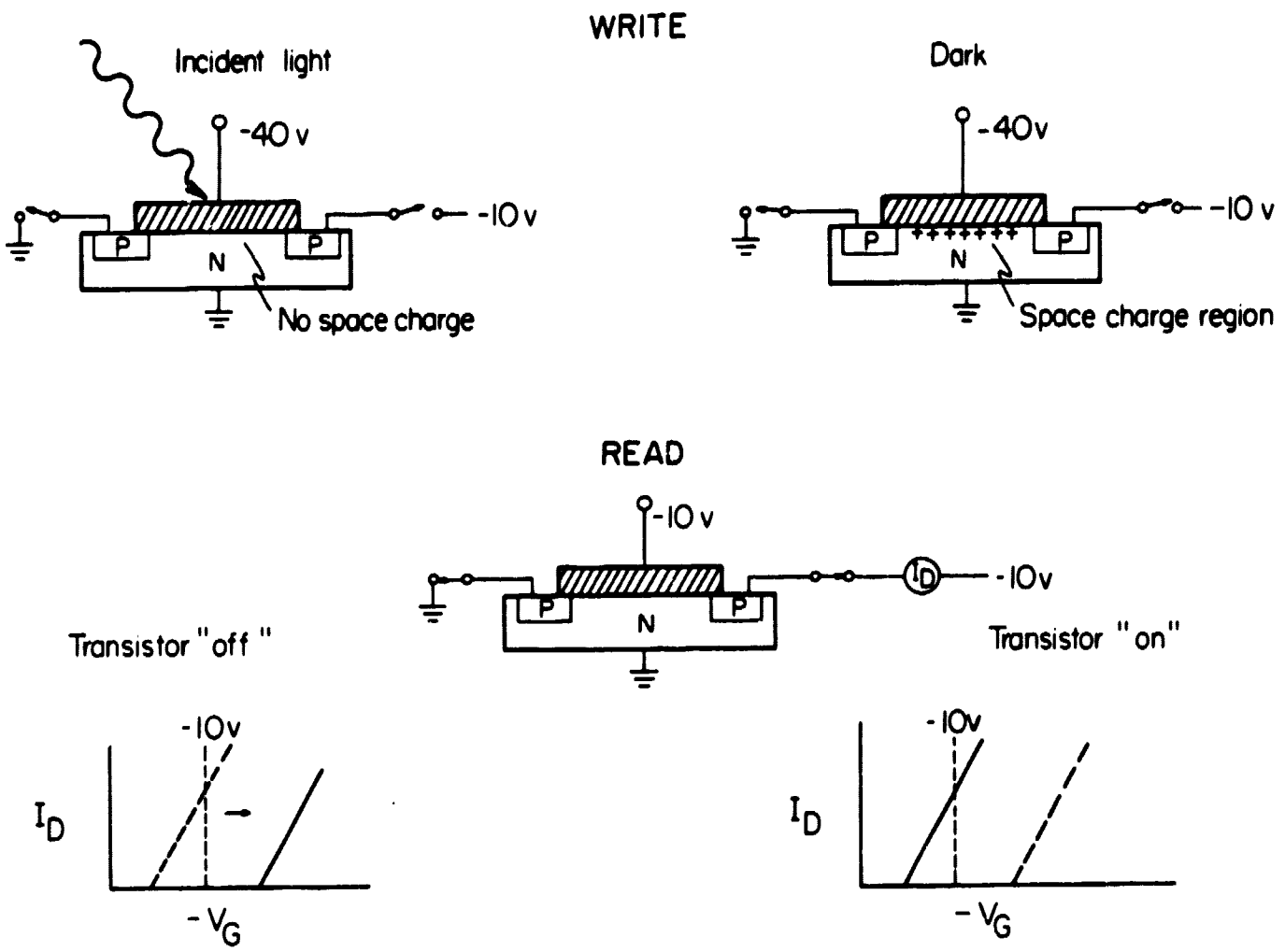

FIG. 6 Operation of MNS light sensitive memory. Shown above, the write cycle for the illuminated and non-illuminated condition. Note floating source and drain. Below, the drain current characteristic is shifted following writing with illumination; shifting is inhibited when writing occurs with no illumination.

minority carriers are generated in the space charge region can be controlled by the intensity of light incident on the silicon space charge region. Light incident on the space charge region generates additional minority carriers which contribute to the collapse of the space charge region. Therefore the light intensity controls the charging time.

Figure 7 demonstrates the results of this phenomenon and indicates how they can be applied to the MNS-VTT light sensing memory element. Here the change in the transistor threshold voltage, ΔV_T, is plotted as a function of pulse width for a constant pulse height with the light intensity as a parameter. Suppose, for example, that a -60 V, 5 msec pulse is used as a write pulse. Then, according to the figure, any light intensity equal to or less than I_3 would have no effect, and any intensity equal to or greater than I_4 would shift the V_T to its maximum value. Thus, it is possible to see how the device, when interrogated with a fixed pulse, would give a "one" or "zero" response, corresponding to a light ($I \geq I_4$) on "no light" I ($I \leq I_3$) condition. On the other hand, an analog response is obtained when the V_T is <u>measured</u> during the interrogation.

The basic measurements shown in Fig. 7 must be accounted for theoretically. In this contract's Sixth Quarterly Technical Report, the equations describing the transient current flow and relating the charge in the system and fields were derived, taking into account the semiconductor space charge region. In this discussion we will show how these equations can be used to calculate charging curves as a function of illumination intensity.

To review briefly, the various charge components that enter into the transient behavior are shown in Fig. 8, where

σ_I = the charge per unit area accumulated at the I_2-I_1 interface

σ_{ss} = the charge per unit area at the I_1-Si interface; voltage dependent states are ignored in this treatment

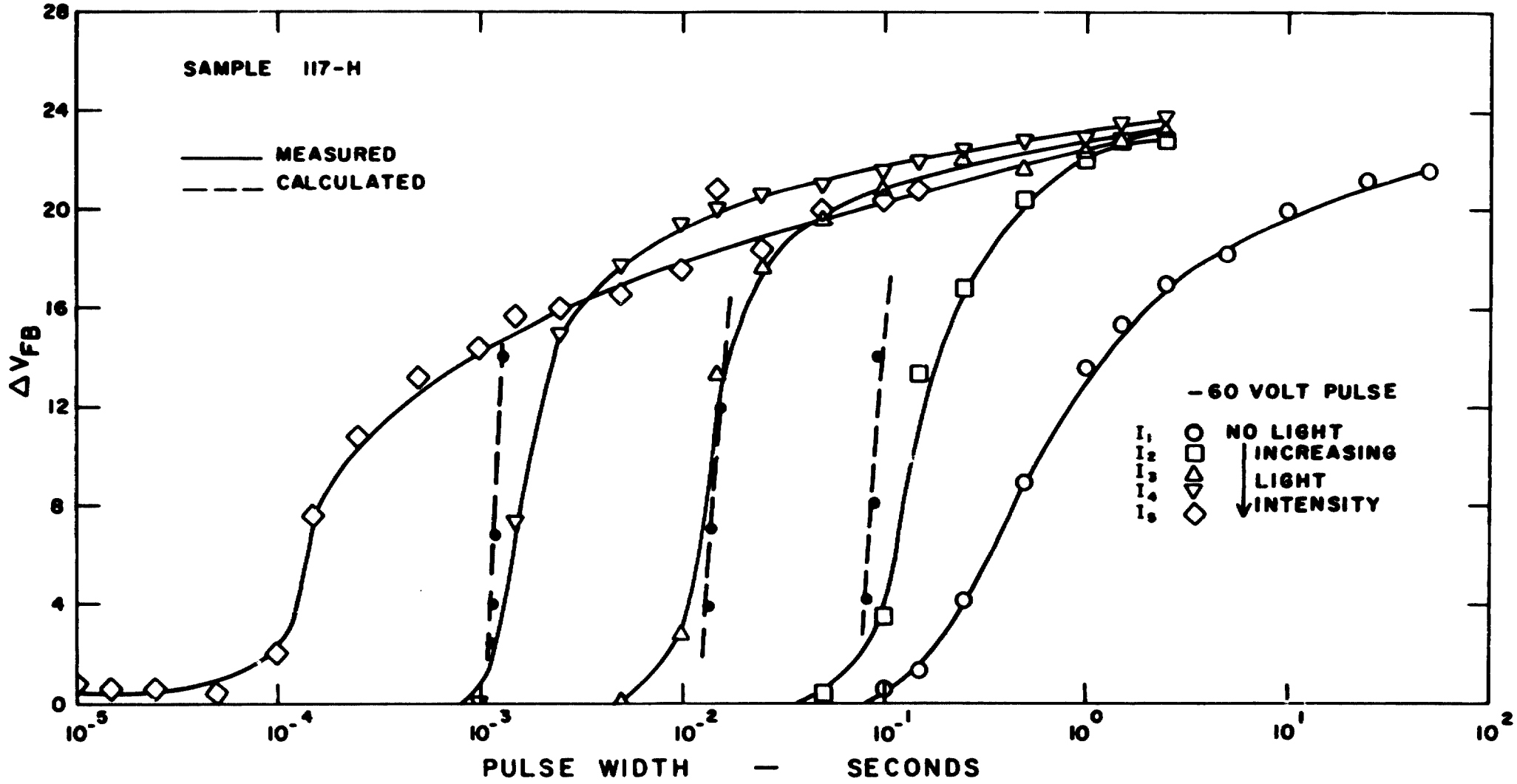

FIG. 7 Charging curves as a function of light intensity.

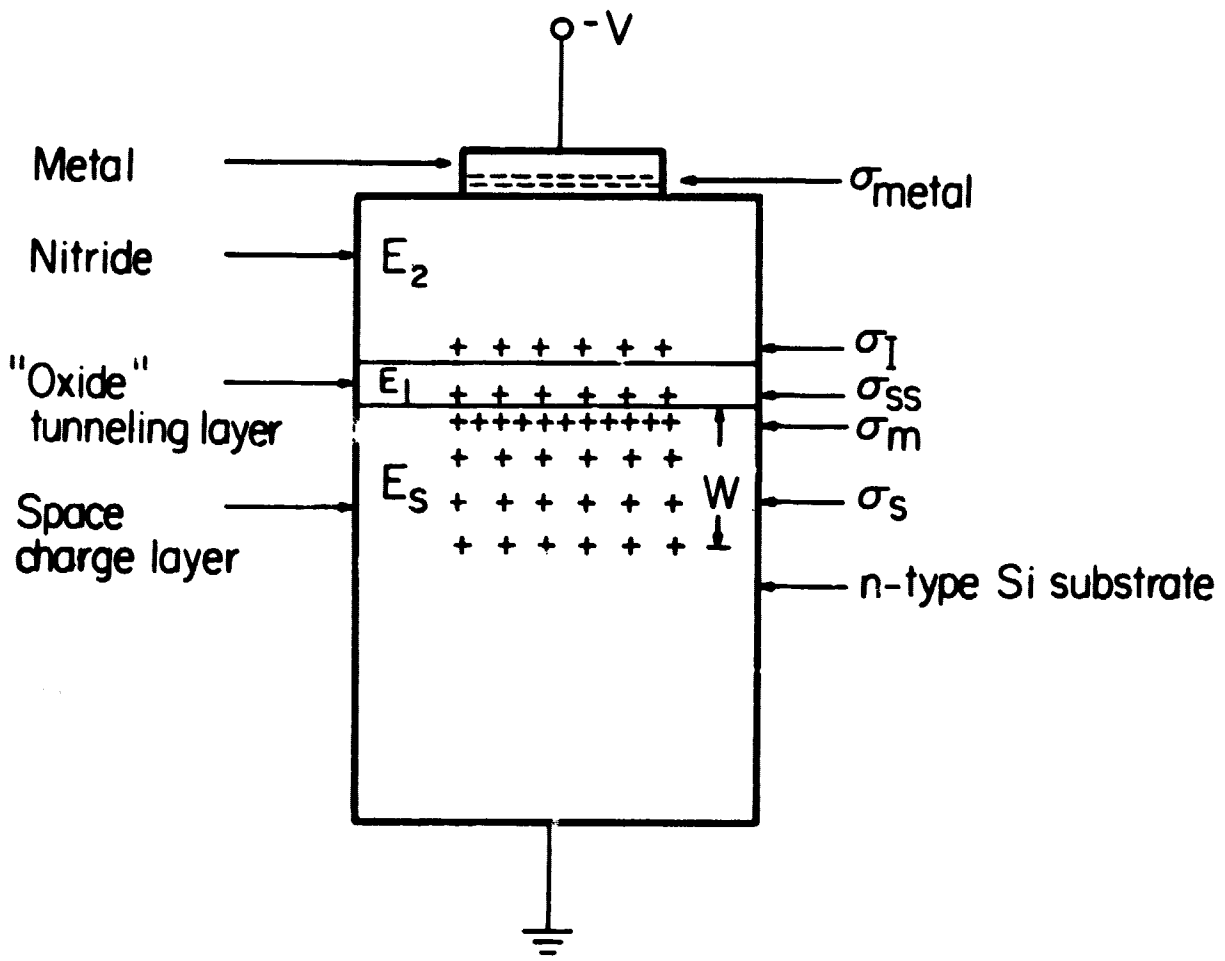

FIG. 8 Charge in MI_2I_1S system.

σ_s - the total charge per unit area due to unneutralized donors or acceptors in the space charge region

σ_m - the charge per unit area due to accumulated minority carriers at the Si-I_1 interface

Assuming that the thickness of the oxide layer is small compared to the thickness of the nitride layer, the solution to Poisson's equation gives the following equations for the oxide field E_1, the nitride field E_2, and the silicon space charge field E_s;

$$E_1 = \frac{1}{\epsilon_1}\left[\sqrt{2}\, G^{\frac{1}{2}}(V_a C_o - \sigma_{ss} - \sigma_I - \sigma_m + \frac{1}{2} G)^{\frac{1}{2}} + \sigma_m + \sigma_{ss} - G\right] \qquad (33)$$

$$E_2 = \frac{1}{\epsilon_2}\left[\sqrt{2}\, G^{\frac{1}{2}}(V_a C_o - \sigma_{ss} - \sigma_I - \sigma_m + \frac{1}{2} G)^{\frac{1}{2}} + \sigma_m + \sigma_{ss} + \sigma_I - G\right] \qquad (34)$$

$$E_s = \frac{1}{\epsilon_s}\left[2\, G^{\frac{1}{2}}(V_a C_o - \sigma_{ss} - \sigma_I - \sigma_m + \frac{1}{2} G)^{\frac{1}{2}} - G\right] \qquad (35)$$

And from the equations of current continuity connecting the three active regions of the device, one obtains the following equations which must be solved simultaneously to obtain the desired charging curve, σ_I or V_{FB} vs time:

$$t = \int \frac{d\sigma_I}{j_1(E_1) - j_2(E_2)} \qquad (36)$$

$$t = \int \frac{d\sigma_m}{j_s(E_s) - j_1(E_1)} \qquad (37)$$

The problem then becomes one of knowing the current field relationships for the three regions, $j_1(E_1)$, $j_2(E_2)$, and $j_s(E_s)$. These conduction

mechanisms cannot be calculated from first principles; therefore they must be extracted experimentally from I-V measurements on the MI_2I_1S structure. We have shown in the Fifth Quarterly Technical Report under this contract, that in a two layer insulator structure (very thin oxide) the $j_1(E_1)$ can be calculated from the static or equilibrium charging behavior of the device. Obtained under proper conditions, any effect due to silicon space charge can be eliminated. The nitride J-E relationship $j_2(E_2)$ can be obtained directly if the oxide layer thickness is negligible in comparison with the nitride thickness.

The remaining problem is that of determining the J-E relationship for the silicon space charge region as a function of illumination intensity. This can be done quite simply by measuring the equilibrium gate current through the MI_2I_1S structure for the polarity that causes the formation of a depletion layer in the silicon. Because current can flow in the insulator, the composite MI_2I_1S device behaves like a hererojunction, and a stable space charge region exists under equilibrium conditions. In the reverse direction, the current is limited by the space charge current. But this current can be determined as a function of the space charge voltage by simply subtracting the voltage for a given current in the forward direction from the voltage for the same current in the reverse direction.

The reverse current curves as a function of light intensity are shown in Fig. 9. The non-limiting curve is simply the Poole-Frenkel conduction due to the nitride layer. It is equivalent to the current in the forward direction. From these curves it is possible to determine the $j_s(E_s)$ relationship, using the appropriate solution to the Poisson Equation to convert the space charge voltage, V_s, to the field E_s.

Thus knowing $j_1(E_1)$, $j_2(E_2)$, and $j_s(E_s)$ the charging behavior can be determined by solving Eqs.(36) and (37) simultaneously. The results are shown by the dashed lines in Fig. 7, where the charging curves for three light intensities were calculated. The agreement with the measured values is good.

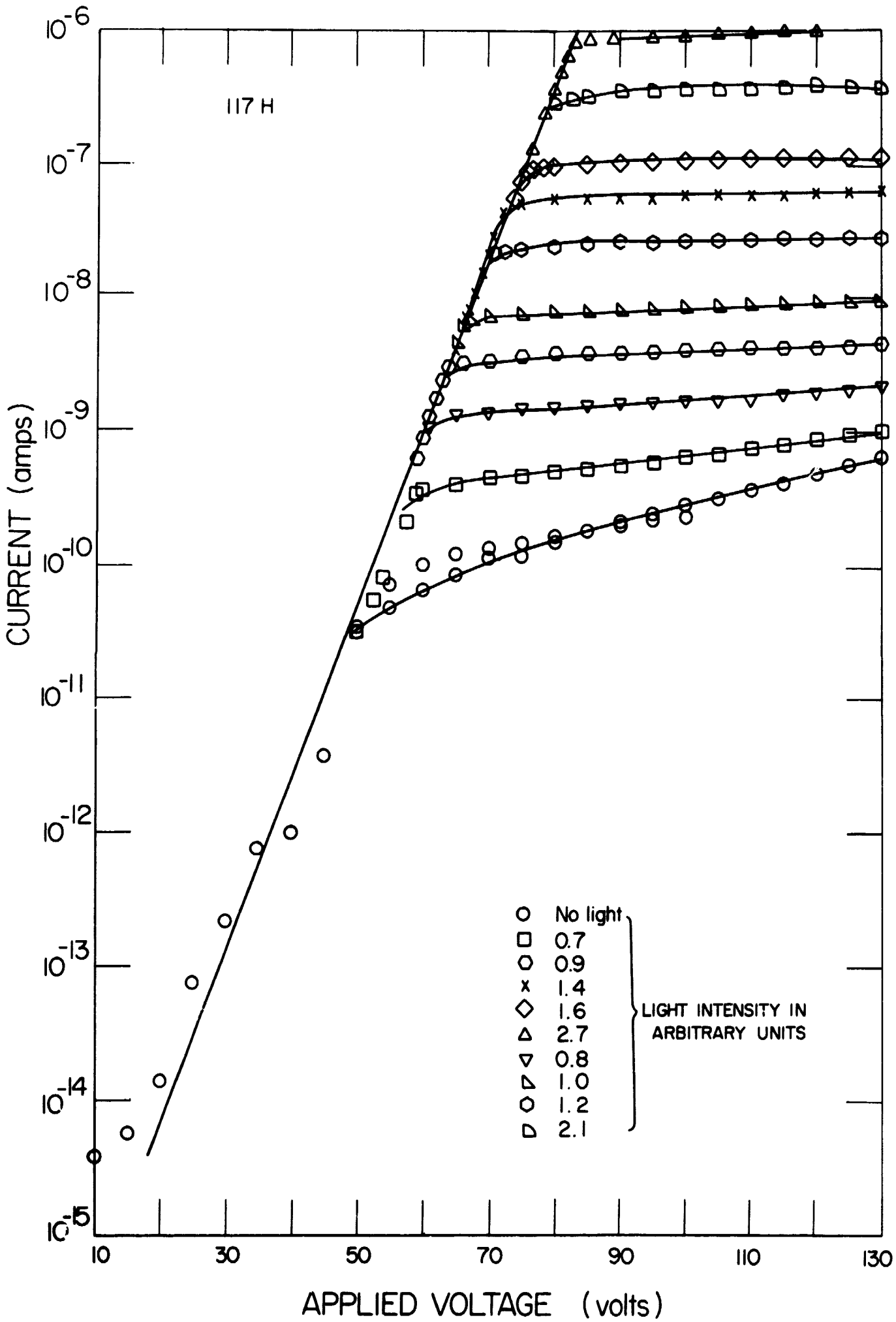

FIG. 9 J-E curves as a function of light intensity. Voltage on gate is negative.

5. Conclusion

During the final period of the contract, experimental confirmation of the decay equations will be attempted. The analysis and experimental confirmation of the decay of stored negative charge will also be considered. It will be important to see if the approximations made in the development of the decay equation for the charge distribution hold. Another important decay measurement is that with a superimposed interrogation field since this is necessary in the practical utilization of this device. Conditions for optimum device performance will be considered. These include the effect of layer thickness variations and that due to multiple layer structures. A particularly interesting structure would be that consisting of a thin silicon oxide layer followed by a thin conductive nitride layer and a relatively thick non-conductive oxynitride layer. This should provide for a well-defined tunnel conduction mechanism between the silicon and the traps in the conductive nitride and a low conductivity mechanism for the decay of charge through the insulator adjacent to the metal gate.

The theoretical equations governing the operation of the new light sensing device have been experimentally confirmed. This device can form the basic element of an image storage array since it has the LSI capability of the MNS-VTT. The present measurements have been performed using electrodes that are relatively opaque. A significant enhancement in light sensitivity can be achieved by using transparent electrodes.

NEW TECHNOLOGY APPENDIX

MNS Light Sensitive Memory Element

On pages 10 through 14 of this report the concept of an MNS light sensitive memory element is described. The behavior is based on the MNS variable threshold transistor, operated in the write mode with the source and drain unconnected. In this way the write voltage is partially dropped across a silicon space charge region, the magnitude of which can be controlled by varying the incident illumination on the device.

We have reported this concept as an invention in the Interim New Technology Report (Contract NAS 12-570, dated July 14, 1969) under the title: "MNS-VTT Light Sensing Memory Element."